Available online at www.sciencedirect.com
SCIENCE DIRECT®
Journal of Solid State Chemistry 176 (2003) 76–87
JOURNAL OF SOLID STATE CHEMISTRY
http://elsevier.com/locate/jssc

Structures of three polymorphs of the complex oxide $K_5Yb(MoO_4)_4$

V.A. Morozov,[a,b] B.I. Lazoryak,[a] O.I. Lebedev,[b,*] S. Amelinckx,[b] and G. Van Tendeloo[b]

[a] *Department of Chemistry, Moscow State University, 119899 Moscow, Russia*
[b] *EMAT, University of Antwerp (RUCA), Groenenborgerlaan 171, B-2020 Antwerp, Belgium*

Received 11 March 2003; received in revised form 5 June 2003; accepted 19 June 2003

Abstract

Polymorphous modifications (γ-, β- and α-) of the double potassium ytterbium molybdenum oxide $K_5Yb(MoO_4)_4$ were synthesized by the solid-state method and their structures were studied by X-ray powder diffraction, electron diffraction and high-resolution electron microscopy. DSC analysis shows that the $\gamma \rightarrow \beta \leftrightarrow \alpha$ phase transitions are not accompanied with a significant reconstruction of the palmierite-type structure. All modifications of $K_5Yb(MoO_4)_4$ are related to the mineral palmierite—$K_2Pb(SO_4)_2$. The palmierite-type structure is made up of isolated AO_4 tetrahedra, which connect the MO_n polyhedra into a 3-D framework via common vertices. Cations occupy two crystallographic positions $M1$ and $M2$. The γ-phase crystallizes in a monoclinic system (space group $C2/c$) with unit-cell parameters: $a = 14.8236(1)$ Å, $b = 12.1293(1)$ Å, $c = 10.5151(1)$ Å, $\beta = 114.559(1)^\circ$, $Z = 4$. The α-phase has space group $R\bar{3}m$ with unit-cell parameters: $a = 6.0372(1)$ Å, $c = 20.4045(2)$ Å. The structures of the γ- and α-modification were refined by the Rietveld method ($R_{wp} = 6.25\%$, $R_I = 2.16\%$ and $R_{wp} = 9.09\%$, $R_I = 5.80\%$ for γ- and α-, respectively). In $K_5Yb(MoO_4)_4$ ytterbium cations occupy $M1$ while K^+ cations occupy $M2$ and $M1$ positions of the palmierite-type structure. In the high-temperature (α-) modification the Yb^{3+} and K^+ occupy the $M1$ site in a statistical manner ($M1 = 0.5Yb^{3+} + 0.5K^+$) while in the low-temperature (γ-) modification these cations occupy this site in an ordered way. The intermediate β-phase shows an incommensurate modulated structure.

Keywords: Complex molybdenum oxides; Polymorphism; Electron microscopy; X-ray diffraction; Incommensurate structure

1. Introduction

The complex molybdenum oxides $M_5R(MoO_4)_4$ (M = Rb, K, Tl; R = rare earth (RE)) are effective phosphors [1–4] characterized by a long lifetime and a high luminescence intensity. For example, the $M_5R_{1-x}Nd_x(MoO_4)_4$ compounds lifetime (τ) is 7.0–7.9×10^{-5} s (at the maximum concentration of Nd^{3+}) and 2.9–3.5×10^{-4} s (at the minimum concentration of Nd^{3+}), respectively [3]. $M_5R(MoO_4)_4$ (M = Rb, K, Tl; R = RE, Y, Bi, Fe, In) [5,6] crystallize in the structure type of a palmierite mineral $K_2Pb(SO_4)_2$ (space group $R\bar{3}m$, $a = 5.49$, $c = 20.83$ Å) [7,8]. The crystal–chemical formula of the palmierite-type structure is $M1^{[6+6]}M2_2^{[9+1]}(AO_4)_2$. Nine varieties of this structure type can be distinguished [6]. The R^{3+} and M^+ cations occupy the $M1$ site in either an ordered or a statistical manner [9,10]. The $M2$ site is occupied by M^+ cations. Projections of the $K_5Sm(MoO_4)_4$ palmierite-type structure on to the ab (a) for $0.10 \leqslant z \leqslant 0.44$ and ac (b) planes are shown in Fig. 1. The palmierite-type structure is built up by [$\cdots - M_2O_{10} - M_1O_{12} - M_2O_{10} - AO_4 - \ AO_4 - \cdots$] columns along the c-axis. These columns form two layers (perpendicular to the c-axis) built of M_1O_{12} polyhedra and AO_4 tetrahedra (layer I) and M_2O_{10} polyhedra (layer II).

Depending on the combinations of elements in these compounds, the structure is subject to different distortions. The coordination number of the $M1$ and $M2$ sites may change. An intrinsic distortion of the ideal palmierite structure will occur for a given compound and composition. The majority of the $M_5R(MoO_4)_4$ compounds crystallizes in the trigonal symmetry of $K_2Pb(SO_4)_2$. A decrease of symmetry to monoclinic or triclinic has been observed for some of them. The distortion of the palmierite-type structure is mainly associated with a rotation of the tetrahedra. The flexibility of the tetrahedra in the palmierite-type structure promotes the formation of coordination polyhedra characteristic of a given trivalent cation.

*Corresponding author. Fax: +32-32180257.
E-mail address: lebedev@ruca.ua.ac.be (O.I. Lebedev).

0022-4596/$ - see front matter © 2003 Elsevier Inc. All rights reserved.
doi:10.1016/S0022-4596(03)00350-5

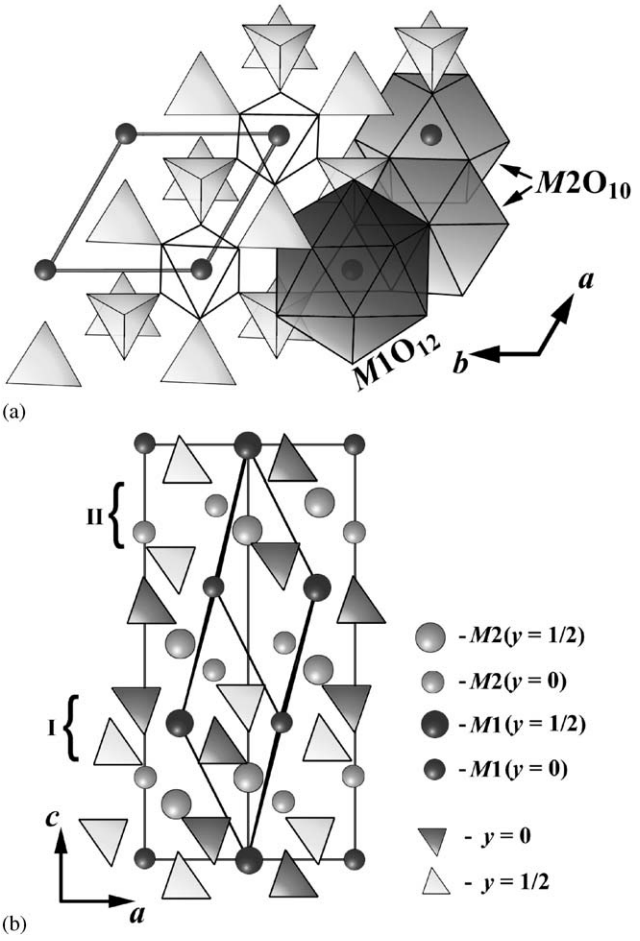

Fig. 1. Projections of the $K_5Sm(MoO_4)_4$ palmierite-type structure on to the *ab* (a) for $0.10 \leqslant z \leqslant 0.44$ and *ac* (b) planes [10].

The ability of the tetrahedra to rotate readily and the occurrence of a low-temperature phase transition in compounds of this type cause the occurrence of ferroelectric and piezoelectric phases [4,11]. It has been established experimentally that in $M_5R(MoO_4)_4$ a low-temperature phase transition occurs in the range 400–895 K [4,11]. For example, a ferroelastic/paraelectric phase transition has been observed in palmierite-type $Pb_3(PO_4)_2$. This transition is accompanied by an increase in the symmetry from monoclinic to trigonal at 453 K [12,13]. The influence of hydrogen insertion on the proton conductivity of single crystals of $Pb_3(PO_4)_2$ is reported in Ref. [14].

The structure of some low-temperature modifications of $M_5R(MoO_4)_4$ (M = Rb, K, Tl; R = rare earth) has not been studied yet. This paper describes the crystal structures of the α-, β- and γ-$K_5Yb(MoO_4)_4$ compounds.

2. Experimental

The low-temperature modification of the complex potassium ytterbium molybdenum oxide (γ-$K_5Yb(MoO_4)_4$) was prepared from an equimolar mixture of K_2CO_3, Yb_2O_3 and MoO_3 by a routine ceramic technique in an Al_2O_3 crucible at 893 ± 10 K for 30 h in air. The intermediate (β-) phase and the high-temperature (α-) modification were synthesized from the γ-$K_5Yb(MoO_4)_4$ phase by heating at 960 ± 10 K (close to the melting point) for 3 h followed by cooling under different conditions. β-$K_5Yb(MoO_4)_4$ was prepared by slowly cooling from 960 ± 10 K to room temperature, while α-$K_5Yb(MoO_4)_4$ was synthesized by quickly quenching from high temperature to liquid nitrogen. A quick quench from 960 ± 10 K to room temperature leads to the formation of the α- and β-modifications mixture.

The X-ray powder diffraction data used for indexing and for the structure refinement of the $K_5Yb(MoO_4)_4$ polymorphous modifications were obtained at room temperature applying the Bragg–Brentano geometry using a Siemens D500 powder diffractometer equipped with a primary SiO_2 monochromator (Cu$K\alpha_1$ radiation, $\lambda = 1.5406$ Å) and a position-sensitive detector (Braun). Structure refinement was performed by the Rietveld method [15] with the RIETAN-94 program [16,17]. The background was refined with a fifth-order polynomial. The peak profile was refined by a modified Pseudo-Voigt function. The electron density maps [$\rho_{exp}(x,y,z)$ and $\Delta\rho_{exp}(x,y,z)$] were calculated using the GSAS program [18].

The second-harmonic generation response of powder samples was measured with a Q-switched YAG:Nd laser at $\lambda_\omega = 1064$ nm, in the reflection mode. The experimental set-up and arrangement have been described elsewhere [19]. Differential scanning calorimetry (DSC) measurements were performed on a NETZSCH STA 409 thermoanalyser in the temperature range from 293 to 1013 K and from 1013 to 493 K (heating/cooling rates were 5 K/min). Sintered kaolin was used as reference material.

Electron diffraction (ED) and high-resolution electron-microscopy (HREM) investigations were made on crushed samples of the various modifications deposited on holey carbon grids. EDX analysis and ED patterns were obtained using a Philips CM20 microscope with a LINK-2000 attachment (analyzed 10–15 crystallites; time of measurements -100 s). HREM observations were performed using a JEOL 4000 EX microscope operating at 400 kV. The Scherzer resolution of the microscope is 1.7 Å. Simulations of the HREM images were performed using the MacTampas software.

3. Results

3.1. General

The elemental content of the 10–15 crystallites for each polymorph of the complex potassium ytterbium

molybdenum oxide was investigated by EDX analysis performed inside the electron microscope. The elemental content is (K—48.3±0.4 (γ-phase), 48.9±0.2 (α-phase), 48.6±0.2 (β-phase) at%; Yb—10.0±0.4 (γ-phase), 10.6±0.2 (α-phase), 9.8±0.2 (β-phase) at%; Mo—41.6±0.6 (γ-phase), 40.4±0.3 (α-phase), 41.6±0.2 (β-phase) at%) and its remains practically constant for all modifications of $K_5Yb(MoO_4)_4$ and reveals a uniform elemental distribution.

The γ-$K_5Yb(MoO_4)_4$ powder sample shows an SHG response, $I_{2\omega}/I_{2\omega}(SiO_2) \sim 0.20$. This significant nonzero SHG response indicates that the γ-modification has a slightly polar structure.

Fig. 2 shows typical heating/cooling DSC curves for γ-$K_5Yb(MoO_4)_4$ obtained at a heating/cooling rate of 5 K/min. The heating/cooling DSC curves indicate the presence of only one peak extending from 938 to 968 K.

The DSC curve obtained on heating exhibits two regions: (1) from 938 to 965 K and (2) from 965 to 973 K (Fig. 2, curve 3). The second temperature region can be associated with the incongruent melting of $K_5Yb(MoO_4)_4$ with the formation of K_2MoO_4 and $KYb(MoO_4)_2$ [20]. These melting temperatures of $K_5Yb(MoO_4)_4$ and $K_2MoO_4 + KYb(MoO_4)_2$ mixture are very close and cannot be separated. A weak broadened peak in the first temperature region can be associated with a shift of structural layers or the $\beta \leftrightarrow \alpha$ phase transition. The DSC investigation shows that the $\gamma \rightarrow \beta \leftrightarrow \alpha$ phase transitions are not accompanied by a significant reconstruction of the palmierite-type structure.

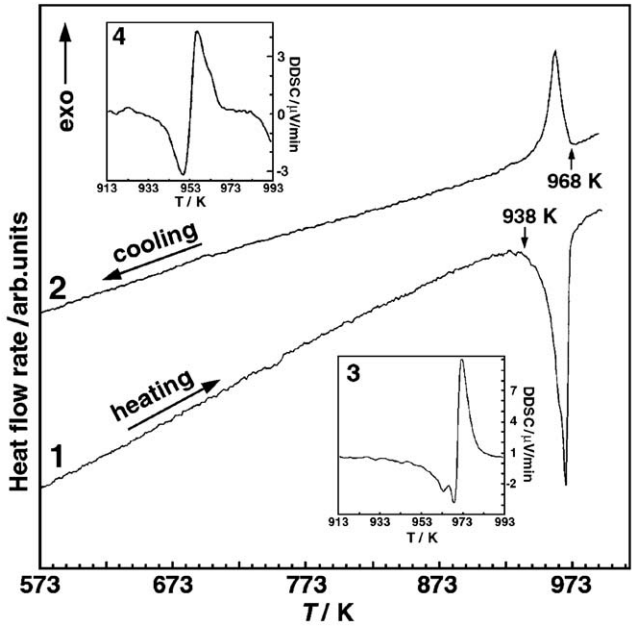

Fig. 2. Heating (1, 3) and cooling (2, 4) DSC (1, 2) and DDSC curves (3, 4) for γ-$K_5Yb(MoO_4)_4$. Heating/cooling rate 5 K/min.

3.2. X-ray powder diffraction

A fragment of the X-ray diffraction patterns for different modifications of $K_5Yb(MoO_4)_4$ are shown in Fig. 3. Experimental data for α-, β-, γ-$K_5Yb(MoO_4)_4$ and for $KYb(MoO_4)_2$ were submitted for JCPDS PDF-2 Data Base, Cards 49–1785, 52–1705, 49–1228 and 50–1762, respectively. It is clear that none of the present XRD spectra contains reflections of the $KYb(MoO_4)_2$ phase.

Mostly the high-temperature α-modification is indexed in an R-centered trigonal unit cell with lattice parameters $a = 6.0379(3)$ Å, $c = 20.406(1)$ Å related to the palmierite ($K_2Pb(SO_4)_2$) subcell by the relations $a_\alpha \approx a_{pal}$, $c_\alpha \approx c_{pal}$. However the X-ray diffraction pattern of α-$K_5Yb(MoO_4)_4$ contains four superstructure reflections with intensities (I) less than 1%: $d = 8.26$ ($I = 0.4$), 4.443 ($I = 0.1$), 4.419 ($I = 0.2$) and 2.4275 ($I = 0.1$). These reflections are indexed in a trigonal unit cell with lattice parameters $a = 10.457$ Å, $c = 20.409$ Å related to the palmierite subcell by $a \approx a_{pal} \times \sqrt{3}$, $c \approx c_{pal}$.

The XRD of the intermediate β-modification is indexed in a C-centered monoclinic unit cell with lattice parameters: $a = 14.143(1)$ Å, $b = 66.923(5)$ Å, $c = 10.391(1)$ Å, $\beta = 106.30°$ related to the α-modification subcell by $a \approx \frac{2}{3}c_\alpha + \frac{1}{3}(b_\alpha - a_\alpha + c_\alpha)$, $b \approx 11b_\alpha$, $c \approx (2a_\alpha + b_\alpha)$. The unexpectedly long lattice parameter b ($b = 66.923(5)$ Å) is a consequence of the incommensurability of the modulation period in the $[010]_\beta$ direction, as will be shown by ED.

3.3. Electron diffraction

3.3.1. α-Phase

ED patterns for α-$K_5Yb(MoO_4)_4$ along the major zones are shown in Fig. 4. The diffraction patterns can be completely indexed in the $R\bar{3}m$ space group using the unit-cell parameters determined from X-ray powder diffraction ($a = 6.0379(3)$ Å, $c = 20.406(1)$ Å). The spots on the $[0001]^*$, $[10\bar{1}0]^*$ and $[\bar{1}101]^*$ diffraction patterns obey the reflection conditions ($-h + k = 3n$ and $-h + k + l = 3n$, respectively), imposed by the $R\bar{3}m$ space group. The $[11\bar{2}0]^*$ diffraction pattern exhibits a rhombohedral shift of the spot rows along c^* over $h \times 1/3c^*$.

The fractional coordinates of $K_2Pb(SO_4)_2$ (palmierite) were used as the initial parameters for the refinement of the α-phase structure. In $K_2Pb(SO_4)_2$ cations occupy two crystallographic positions $M1$ (Pb) and $M2$ (K). In α-$K_5Yb(MoO_4)_4$ potassium cations occupy the $M2$ position of the palmierite-type structure while the $M1$ positions are statistically occupied by K^+ and Yb^{3+} ($M1 = 0.5K^+ + 0.5Yb^{3+}$). The anion positions are fully occupied by MoO_4^{2-} tetrahedra. The occupancy factor for the $M2$ site by K^+ cations and of the $M1$ site

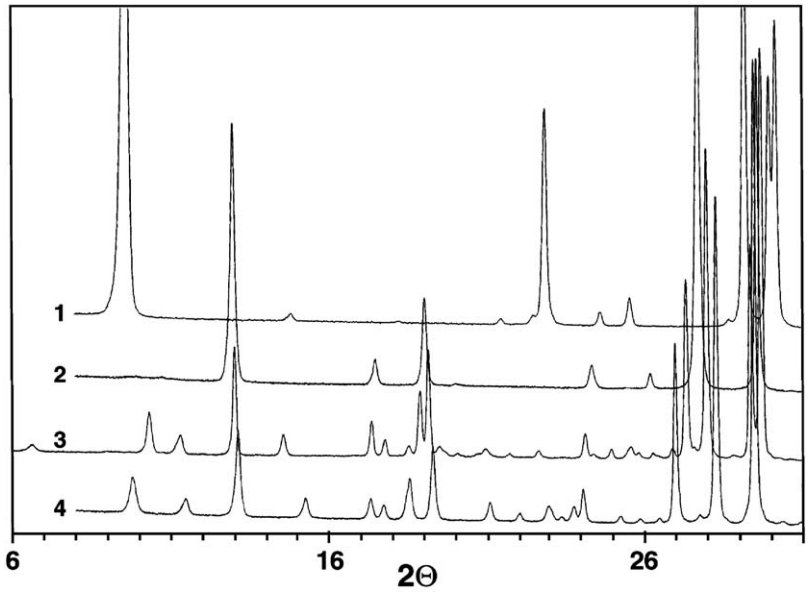

Fig. 3. Fraction of the X-ray diffraction patterns of $KYb(MoO_4)_2$ (1) and of the different modifications of $K_5Yb(MoO_4)_4$ (2—α, 3—β, 4—γ).

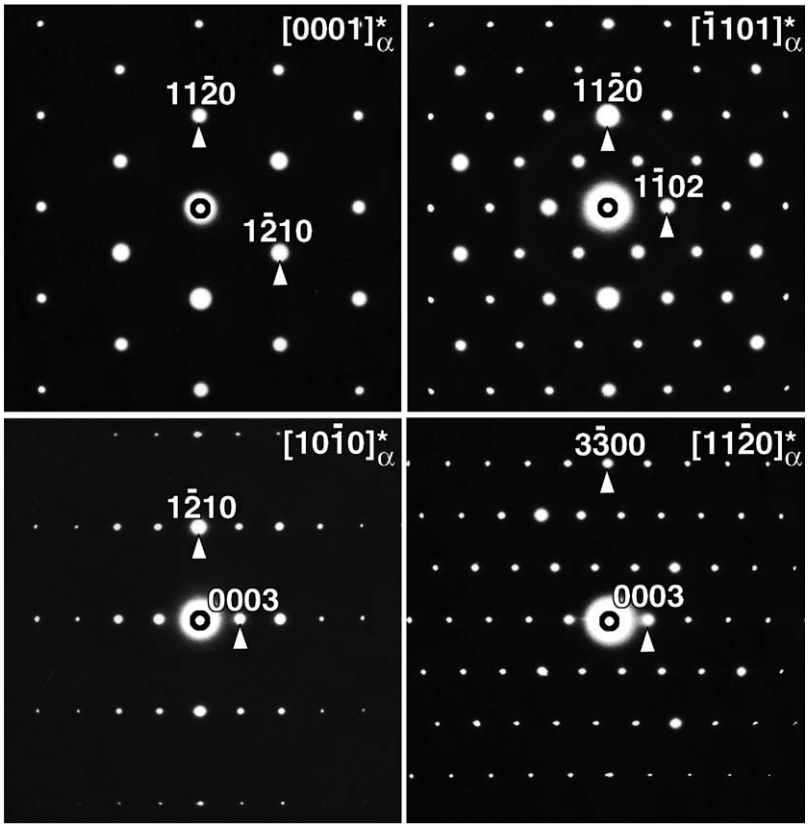

Fig. 4. Electron diffraction patterns of α-$K_5Yb(MoO_4)_4$ along the main zone axes.

($M1 = 0.5K^{+} + 0.5Yb^{3+}$) can be refined but does not deviate significantly from full occupation.

After refinement of α-$K_5Yb(MoO_4)_4$ structure in the $K_2Pb(SO_4)_2$ model the isotropic atomic displacement parameters for oxygen atoms O1 (site symmetry 6*c*) and O2 (site 18*m*) were $B_{iso.} = 8.9(4)$ and 8.8(3), respectively. In the $K_2Pb(SO_4)_2$ structure O1 and O2 oxygen atoms lie on the three-fold axis and on a plane perpendicular to this axis, respectively. It should be noted that higher isotropic atomic displacement parameters for oxygen

atoms can be associated with a displacement of the oxygen from the three-fold axis (O1) and the special position (x, $\bar{x}$, z) (O2). Indeed such oxygen displacements were observed for the potassium yttrium molybdenum oxide with the palmierite-type structure [21]. Fig. 5 shows the $[\rho_{exp}.(x,y,z)]$ electron density plots of α-$K_5Yb(MoO_4)_4$ for the (001) (a, b) and (010) (c) planes through the O2 (a) and O1 (b, c) atoms. The spherical electron density of the oxygen atoms and the absence of residual density show that a displacement of the oxygen atoms is not observed here.

After the last refinement there is a good agreement between the observed and calculated pattern. Details of data collection and refinement are given in Table 1. The final atomic parameters are listed in Table 2. Table 3 presents selected interatomic distances and angles in the MoO_4^{2-} tetrahedron. A part of the Rietveld profile for α-$K_5Yb(MoO_4)_4$ is shown in Fig. 6.

3.3.2. γ -Phase

The $[001]^*_\gamma$, $[100]^*_\gamma$, $[010]^*_\gamma$ and $[302]^*_\gamma$ ED patterns for γ-$K_5Yb(MoO_4)_4$ are shown in Fig. 7. The relation between the unit-cell vectors of the rhombohedral (α-modification) and the monoclinic unit cell (γ-modification) is as follows: $[10\bar{1}0]^*_\alpha = [001]^*_\gamma$, $[0001]^*_\alpha = [302]^*_\gamma$, $[\bar{1}101]^*_\alpha = [100]^*_\gamma$ and $[11\bar{2}0]^*_\alpha = [010]^*_\gamma$. The difference between the rhombohedral and the monoclinic modification is the appearance of superstructure reflections in the $[001]^*_\gamma$, $[100]^*_\gamma$, and $[302]^*_\gamma$ zones and the deviation from 90° of the angle between the 2 0 0 and $\bar{4}$ 0 6 in the $[010]^*_\gamma$ ED pattern; the corresponding angle between the $0\,0\,0\,l$ and the $h\,\bar{h}\,0\,0$ rows in the $[11\bar{2}0]^*_\alpha$ pattern for the α-modification (Fig. 4) is equal to 90°.

The ED patterns for γ-$K_5Yb(MoO_4)_4$ can be completely indexed in the Cc or $C2/c$ space group using the unit-cell parameters determined from X-ray powder diffraction. The spots on the $[001]^*_\gamma$ diffraction pattern obey the extinction conditions $h\,k\,0$, $h+k=2n$ and indicate the presence of a C-centered unit cell. The $[100]^*_\gamma$ pattern exhibits $0\,0\,l$, $l \neq 2n$ reflections forbidden by the Cc or $C2/c$ symmetries. However, the intensity of these reflections is systematically lower than the intensity of $0\,0\,l$, $l=2n$. Upon tilting the sample around the $0\,0\,l$ row the reflections with $l \neq 2n$ weaken and finally vanish. The appearance of these forbidden reflections has to be attributed to double diffraction. The $0\,0\,l$, $l \neq 2n$ reflections are absent in the $[010]^*_\gamma$ zone since the conditions for double diffraction are not present. The $h\,0\,l$, h, $l=2n$ and $h\,k\,l$, $h+k=2n$ reflection conditions are observed in the $[010]^*_\gamma$ and $[302]^*_\gamma$ diffraction patterns, respectively.

Analysis of the reflection positions in the XRD of the γ-phase has shown that this modification is isotypic with monoclinic distorted β-$K_5In(MoO_4)_4$ (space group Cc, $Z=4$, $a=14.625$ Å, $b=12.092$ Å, $c=10.46$ Å, $\beta=114.0°$) [22]. In β-$K_5In(MoO_4)_4$ cations

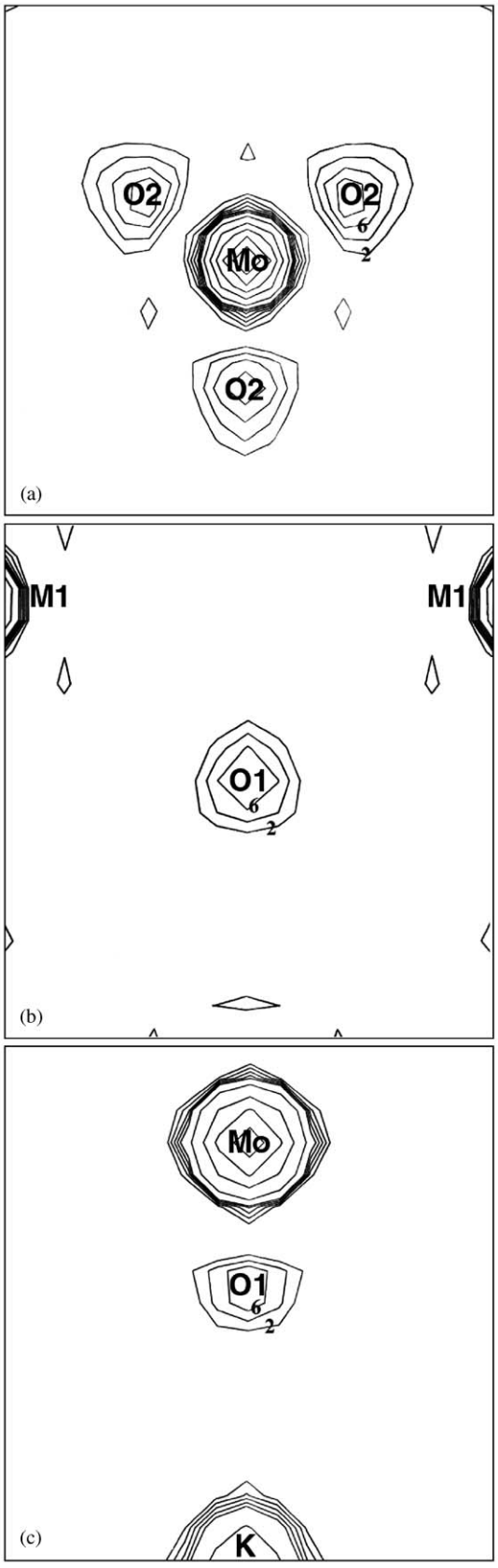

Fig. 5. $[\rho_{exp}.(x,y,z)]$ electron density plots for α-$K_5Yb(MoO_4)_4$ in the (001) (a, b) and (010) (c) planes through O2 (a) and O1 (b, c) atoms. The contour line values for oxygen atoms (e/Å^3) have been marked.

Table 1
Crystallographic data, recording conditions and refinement results for different modifications of $K_5Yb(MoO_4)_4$

	γ-Phase	α-Phase
Temperature (K)	297	297
Space group	$C2/c$	$R\bar{3}m$
2Θ range (°)	8–110	8–110
Step scan increment (2Θ)	0.01	0.01
I_{max}	71 782	66 206
Unit-cell parameters		
a (Å)	14.8236(1)	6.0372(1)
b (Å)	12.1293(1)	
c (Å)	10.5151(1)	20.4045(2)
β (Å)	114.559(1)	
V (Å^3)	1719.58(3)	644.06(1)
Z	4	1.5
Number of reflections	1084	126
Reliable factors[a]		
R_{wp}, R_P	6.25%, 4.74%	9.09%, 6.67%
R_I, R_F	2.16%, 1.21%	5.80%, 3.06%

[a] Refined as in Ref. [16].

Table 2
Fractional atomic coordinates and thermal parameters for α-$K_5Yb(MoO_4)_4$

Atom	Site	x	y	z	Biso
M[a]	3a	0.0	0.0	0.0	0.98(4)
K	6c	0.0	0.0	0.1954(2)	3.6(1)
Mo	6c	0.0	0.0	0.3989(1)	1.09(4)
O1	6c	0.0	0.0	0.3181(5)	8.9(4)
O2	18h	−0.1694(6)	0.1694(6)	0.4111(2)	8.8(3)

[a] $M = 0.5Yb + 0.5K$.

Table 3
Interatomic distances (Å) and angles (°) in α-$K_5Yb(MoO_4)_4$

Distance	Å	Distance	Å
M–O12 × 6	2.2336(5)	K–O11	2.504(10)
M–O11 × 6	3.499(1)	K–O12 × 3	2.950(7)
		K–O12 × 6	3.259(2)
⟨M–O⟩	2.866	⟨K1–O⟩	3.091
MoO_4-tetrahedron	O11	O12	O12
O11	1.649(10)	98.0(2)	98.0(2)
O12		1.788(7)	118.10(7)
O12			1.788(7)

occupy six (four-fold) crystallographic positions with five potassium sites. The K2–K5 potassium positions are structurally related to the $M2$ position while the R^{3+} and K1 positions are structurally related to the $M1$ position of the palmierite-type structure. In this structure indium and potassium occupy the $M1$ site in an ordered manner.

The fractional coordinates in β-$K_5In(MoO_4)_4$ were used as initial parameters for the refinement of the γ-phase. SHG data show that the structure of the γ-modification is slightly polar. Examination of the atom positions in the β-$K_5In(MoO_4)_4$ structure model (space group Cc) shows that the distribution of the majority of the atoms is close to centrosymmetric. For this reason the structure of γ-$K_5Yb(MoO_4)_4$ was refined in the $C2/c$ space group. In this model the four-fold K2 and K4, K3 and K5 sites as well as the $Mo1O_4$ and $Mo3O_4$, $Mo2O_4$ and $Mo4O_4$ tetrahedra of the β-$K_5In(MoO_4)_4$ structure are equivalent.

After the last refinement in the $C2/c$ model there is good agreement between the observed and the calculated pattern and reasonable values of isotropic atomic displacement parameters were found for all atoms. The refinement of the structure in the polar Cc did not lead to a significant decrease of the R-factors ($R_{wp} = 6.14$, $R_I = 2.08$). But in this case the number of refinement parameters for the atoms doubles and a strong correlation for the majority of the atomic (K, Mo and O) position parameters was observed.

Details of the data collection and the refinement are given in Table 1. The final atomic parameters are listed in Table 4. Table 5 presents the interatomic distances and angles in the tetrahedra. Part of the Rietveld profile for γ-$K_5Yb(MoO_4)_4$ is shown in Fig. 8.

3.3.3. β-Phase

The $[001]^*_\beta$, $[100]^*_\beta$, $[010]^*_\beta$ and $[301]^*_\beta$ ED patterns for intermediate β-$K_5Yb(MoO_4)_4$ are shown in Fig. 9. XRD only allows to index the basic reflections based on a C-centered monoclinic structure The ED patterns of the β-phase are clearly incommensurate which explain the problems to determine the exact structure from X-ray data. An interpretation of the ED patterns and a proposed structure based on ED and HREM data will be given below.

To describe the structure of the intermediate β-phase we will first introduce a schematic model of the ordered low-temperature γ-phase. We focus our attention on the pairs of K-columns and the corresponding AO_4 tetrahedra shown for the α-phase in Fig. 10a. Changes in inclination of some of the segments clearly imply rearrangements of all other atoms in the structure. The choice of the K-ions as a representative of the whole structure is justified by the full occupancy of these sites in the γ-phase and the statistical occupation in the α-phase. The γ-phase is represented in Fig. 10b. and the intermediate β-phase can then be represented as in Fig. 11. This representation suggests models for interfaces with a displacement vector of the type $1/4[010]_\gamma$. Since the observed period of the β-phase (i.e. $1/q$) along [010] is somewhat smaller than that of the γ-phase, it is suggested that interfaces such as in Fig. 11 regularly occur in the β-phase leading to a somewhat reduced

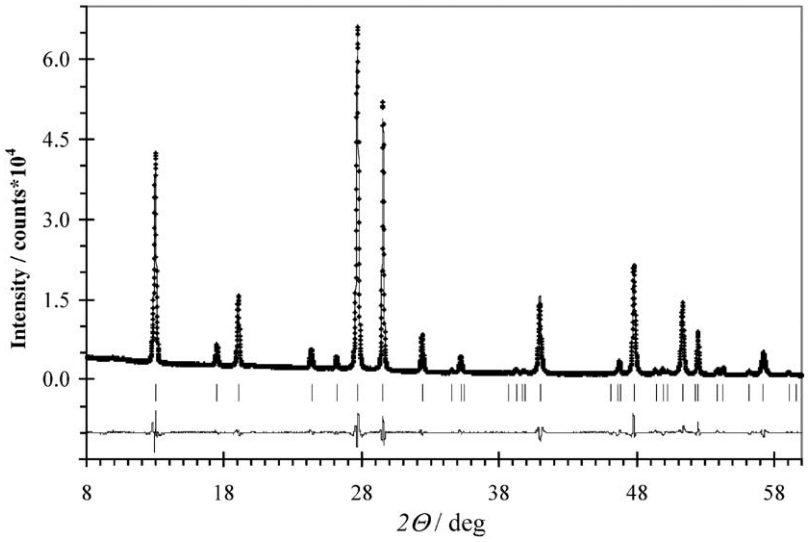

Fig. 6. Observed (crosses), calculated (solid line), and difference XRD patterns in a 2θ range of $8-60^\circ$ for α-$K_5Yb(MoO_4)_4$. Tick marks denote the peak positions of possible Bragg reflections.

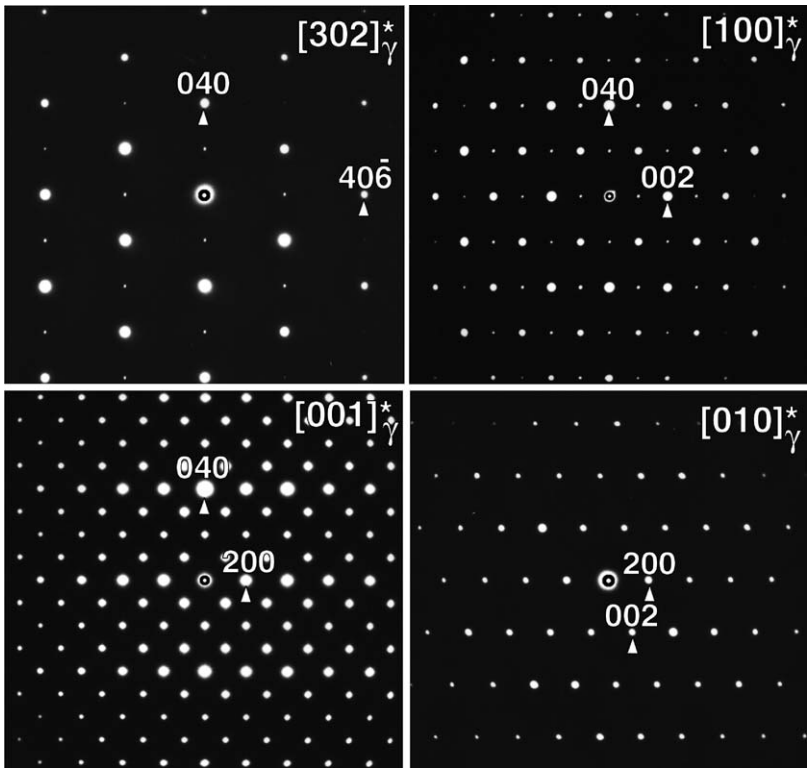

Fig. 7. The $[001]^*_\gamma$, $[100]^*_\gamma$, $[010]^*_\gamma$ and $[302]^*_\gamma$ ED patterns for γ-$K_5Yb(MoO_4)_4$.

average period which is incommensurate with the corresponding period of the γ-phase.

3.4. High-resolution electron microscopy

A HREM study has been performed along the most informative [001] and $[10\bar{1}0]$ directions where the structure can be simply interpreted in terms of cation and oxygen columns. The contrast interpretation has been carried out by comparing the experimental images with calculated ones. The positional parameters of α-$K_5Yb(MoO_4)_4$ obtained from the X-ray powder refinement were taken as an input for the image calculations.

Table 4
Fractional atomic coordinates and thermal parameters for γ $K_5Yb(MoO_4)_4$

Atom	Site	x	y	z	B_{iso}
Yb	4*e*	0.0	0.1190(2)	0.25	0.98(4)
K1	4*e*	0.5	0.1132(7)	0.25	3.9(2)
K2	8*f*	0.2941(3)	0.3714(6)	0.9320(4)	2.7(1)
K3	8*f*	0.2841(3)	0.8944(5)	0.9401(5)	2.8(2)
Mo1	8*f*	0.1035(1)	0.3680(2)	0.1550(2)	1.15(5)
O11	8*f*	0.9863(9)	0.4027(11)	0.0753(12)	3.7(4)
O12	8*f*	0.1654(9)	0.4690(9)	0.2752(12)	2.3(3)
O13	8*f*	0.1495(6)	0.3797(12)	0.0305(9)	1.9(3)
O14	8*f*	0.1126(9)	0.2328(8)	0.2327(11)	1.3(3)
Mo2	8*f*	0.0913(1)	0.8667(2)	0.1390(2)	0.97(4)
O21	8*f*	0.9741(8)	0.8216(8)	0.0992(11)	0.7(3)
O22	8*f*	0.1056(6)	0.8914(11)	0.9894(9)	2.1(3)
O23	8*f*	0.0959(9)	0.9839(9)	0.2324(12)	3.5(4)
O24	8*f*	0.1662(8)	0.7649(9)	0.2342(13)	1.6(3)

Table 5
Interatomic distances (Å) and angles (°) in γ-$K_5Yb(MoO_4)_4$

Distance	Å	Distance	Å	
Yb–O23 × 2	2.226(12)	K1–O13 × 2	2.861(9)	
Yb–O14 × 2	2.231(11)	K1–O21 × 2	2.923(11)	
Yb–O22 × 2	2.351(9)	K1–O12 × 2	2.934(12)	
⟨Yb–O⟩	2.27	K1–O11 × 2	3.103(15)	
		K1–O24 × 2	3.135(12)	
		K1–O11 × 2	3.515(11)	
		⟨K1–O⟩	3.08	
K2–O21	2.580(15)	K3–O11	2.730(12)	
K2–O24	2.716(13)	K3–O13	2.883(15)	
K2–O13	2.742(9)	K3–O22	2.900(9)	
K2–O12	2.738(13)	K3–O12	2.912(11)	
K2–O14	2.915(12)	K3–O24	2.959(13)	
K2–O13A	3.140(15)	K3–O14	2.999(12)	
K2–O22	3.210(12)	K3–O23	3.110(13)	
K2–O23	3.328(12)	K3–O12A	3.137(12)	
K2–O23A	3.491(12)	⟨K3–O⟩	2.95	
⟨K2–O⟩	2.98			
$Mo1O_4$-tetrahedron	O11	O12	O13	O14
O11	1.639(12)	108.7(6)	105.2(5)	109.1(6)
O12		1.724(12)	104.0(6)	113.3(5)
O13			1.716(9)	116.1(6)
O14				1.813(11)
$Mo2O_4$-tetrahedron	O21	O22	O23	O24
O21	1.670(11)	109.7(4)	101.6(5)	105.3(5)
O22		1.699(9)	113.2(6)	112.0(6)
O23			1.713(11)	114.1(5)
O24				1.684(12)

Fig. 12 shows an HREM image of α-phase along the $[\bar{1}101]$ zone where the bright dots in the HREM image correspond to the K atom column while less bright correspond to column wiith mixture of K and Yb atoms. The calculated images are given as an inset and show a good agreement with the experimental images.

Fig. 13 shows $[10\bar{1}0]$ and [001] images of the α-, and β-modifications, respectively, corresponding with the diffraction patterns of Figs. 4 and 9. These images reflect the main geometrical features of the layer stacking according to the structure schematically represented in Figs. 10a and 11.

4. Discussion

All modifications of the complex potassium ytterbium molybdenum oxide ($K_5Yb(MoO_4)_4$) are based on the palmierite-type structure [7,8]. The palmierite-type structure is made up of isolated AO_4 tetrahedra, which connect the MO_n polyhedra into a 3-D framework via common vertices. Cations occupy the two crystallographic positions $M1$ and $M2$. In the $K_2Pb(SO_4)_2$ structure the Pb^{2+} cations occupy the $M1$, while the K^+ occupy the $M2$ position of the palmierite structure. All layers in the palmierite-type structure along $[11\bar{2}0]$ are built up by columns which can be presented as $[\cdots-M_2O_{10}-M_1O_{12}-M_2O_{10}-AO_4-AO_4-\cdots]$. The 3-D framework can be described as made up of two layers (perpendicular to the c-axis) built of M_1O_{12} polyhedra and AO_4 tetrahedra (layer I) and M_2O_{10} polyhedra (layer II). Moreover two I layers are separated by two II layers (Fig. 10a).

In $K_5Yb(MoO_4)_4$ ytterbium cations occupy $M1$ while K^+ cations occupy $M2$ and $M1$ positions. In the high-temperature α-modification Yb^{3+} and K^+ occupy the $M1$ site in a statistical manner ($M1 = 0.5Yb^{3+} + 0.5K^+$) (Fig. 10a) while in the low-temperature γ-modification these cations occupy the $M1$ site in an ordered manner (Fig. 10b). Two Yb columns alternate with two potassium columns. Cation ordering in the layers I and the rotation of the MoO_4^{2-} tetrahedra lead to a zig-zag deformation of the MoO_4^{2-} layers in the γ-modification as compared with the α-modification.

The thermal treatments by which the α- and β-phases are produced from the γ-phase suggest that the structure of these phases should be topologically related. Their close relationship is clearly illustrated by the similarity of the geometry and the intensity distribution of the diffraction patterns along the topologically corresponding zone axes. The most convincing example is provided by the corresponding zones of the α-, β- and γ-phases represented schematically in Fig. 14. The γ-phase pattern exhibits the same rectangle of intense basic spots as the α-phase, but moreover it shows weaker "superstructure" spots (Fig. 14b). These zone patterns reflect the main features of the geometry of the layer stacking as seen along the K-columns according to the structure determined by X-ray diffraction.

The ED pattern of the β-phase (Fig. 14a) is incommensurate. It can be described as consisting of a short array of equidistant spots with a spacing q^*

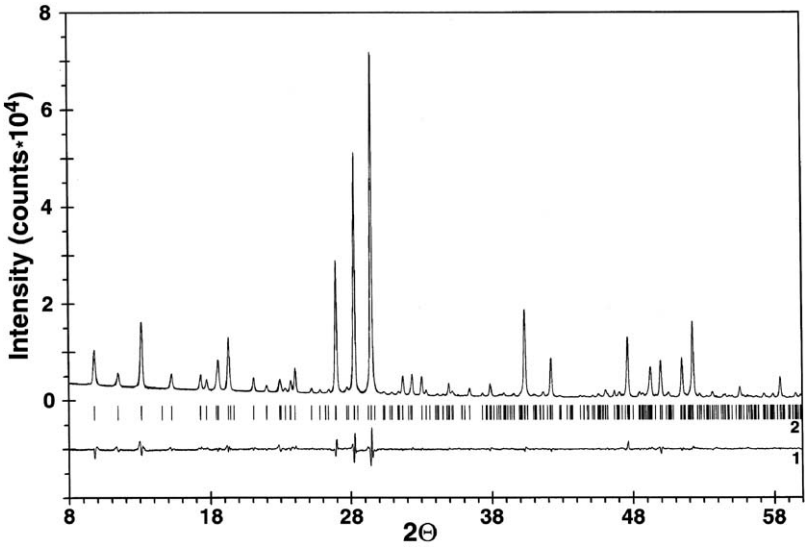

Fig. 8. Observed (crosses), calculated (solid line), and difference XRD patterns in the 2θ range $8-60^\circ$ for γ-$K_5Yb(MoO_4)_4$. Marks denote the peak positions of possible Bragg reflections.

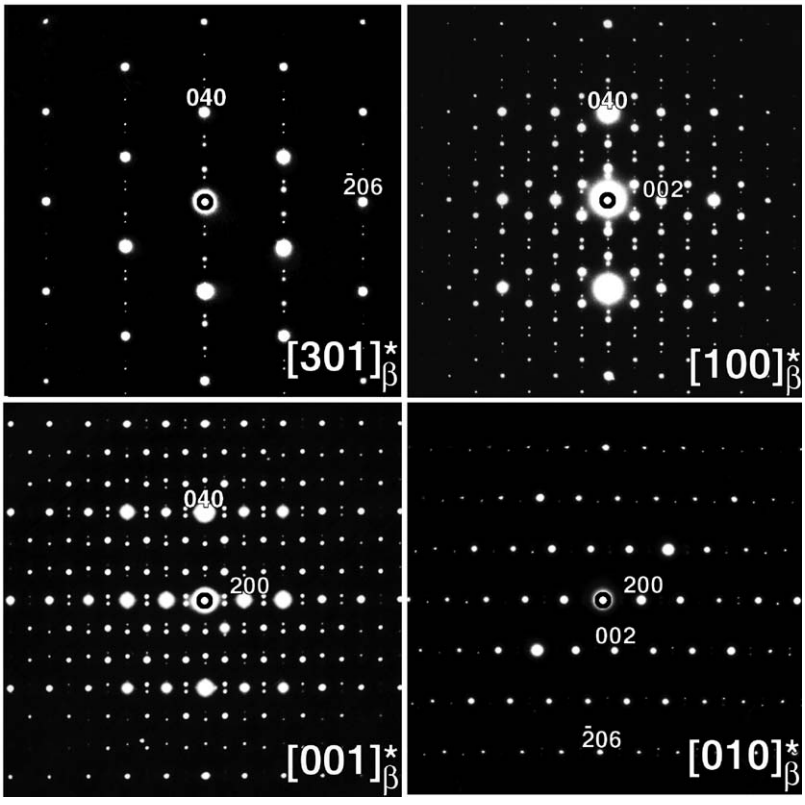

Fig. 9. $[001]^*_\beta$, $[100]^*_\beta$, $[010]^*_\beta$ and $[301]^*_\beta$ ED patterns of β-$K_5Yb(MoO_4)_4$.

(see schematic representation of Fig. 14a). Each array is associated with a spot position of the γ-phase. These positions are indicated by crosses in the schematic representation of Fig. 14a. The equidistant spot arrays of the β-phase are shifted with respect to the γ-phase positions over a fraction of their spacing q^*. These "fractional shifts", with a magnitude depending on the associated γ-position, are indicated in Fig. 14a. Such linear spot arrays with fractional shifts are characteristic of interface modulated structures (see e.g. Ref. [23]).

The pattern of Fig. 14a and in particular the relationship with the α- and β-phase suggest that the

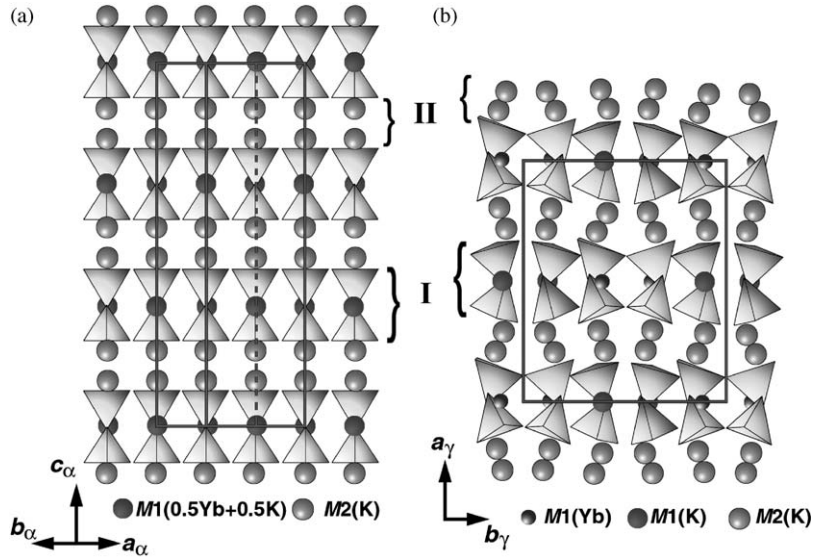

Fig. 10. Projection of the α-$K_5Yb(MoO_4)_4$ (a) on the $(11\bar{2}0)$ plane and γ-$K_5Yb(MoO_4)_4$ (b) on the (001) plane. Layers II and I have been marked.

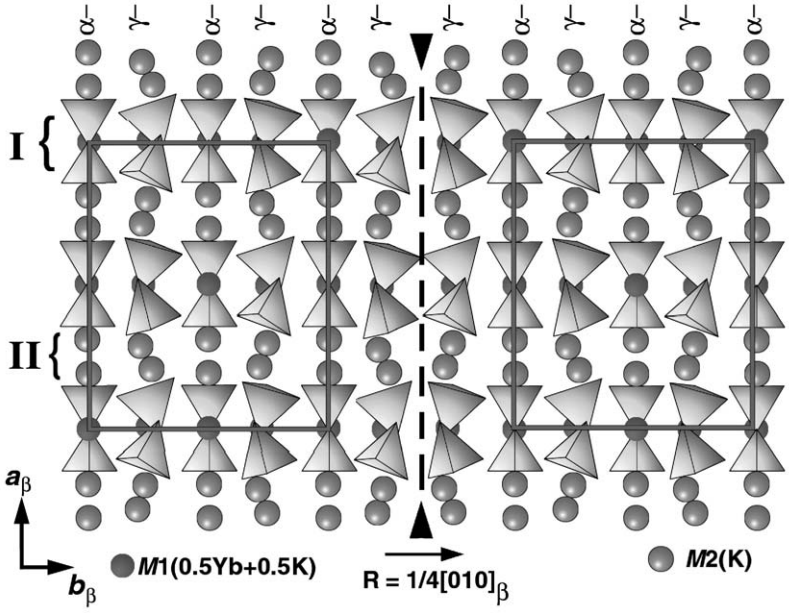

Fig. 11. Model for β-$K_5Yb(MoO_4)_4$.

β-phase could be interpreted as an interface modulated superstructure consisting of strips of the γ-structure limited by parallel interfaces perpendicular to $[010]_\gamma$ and along which the γ-structures on both sides of the interface are shifted over a vector $\bar{R}_o$ which determines the fractional shift.

A summary of the diffraction theory of interface modulated structures is given in Ref. [23]. The geometry of the diffraction pattern is characterized by the relation

$$\bar{H} = \bar{h} + (m - \bar{h}.\bar{R})\bar{q},$$

where $\bar{H}$ is the diffraction vector of the superstructure spot; $\bar{h}$ the diffraction vector of the "basic" structure spot; $\bar{R}$ the displacement vector of the interfaces separated by $d = 1/q$; m the (integer) order of the superstructure spot in the array; the spot intensity decreases rapidly with increasing order; $\bar{q}$ the wave vector of the modulated structure $\bar{q} = 1/d\ (\bar{e}_n)$; $\bar{h}.\bar{R}$ the fractional shift of the spot array.

The observed fractional shifts give information on the projection of the R vector on the various diffraction vectors $\bar{h}$. Representing $\bar{R}$ as $[uvw]$ and $\bar{q} = [hkl]$ the

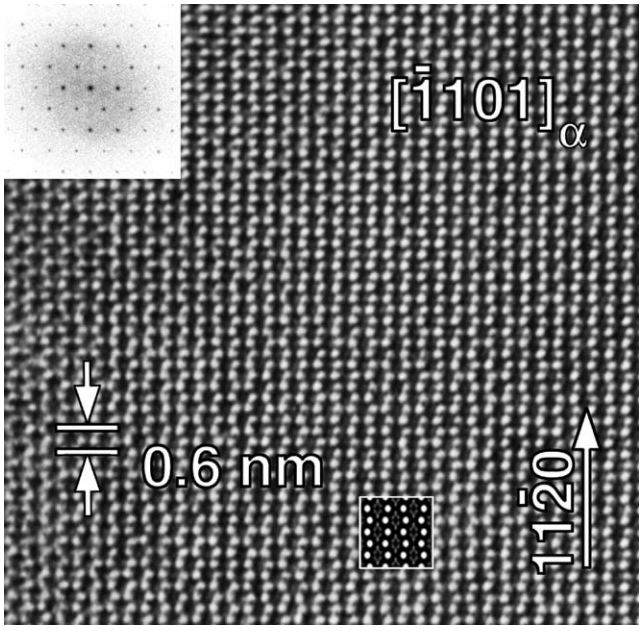

Fig. 12. HREM image of α-$K_5Yb(MoO_4)_4$ along the [1̄101] zone. The calculated image for a defocus value $\Delta f = -10$ nm and a thickness $t = 4$ nm is given as inset.

observations lead to $\bar{R} = [0\,??\,w]$; the third component cannot be deduced from this pattern.

In the present case the "basic" structure is the γ-structure represented in Fig. 10b. We note in particular that the repeated distance along $[010]_\gamma$ (i.e. 1.212 nm) contains four columns formed by the projections of zig-zag chains of potassium ions in inclined planes. The repeat period along $[010]_\gamma$ can thus be associated with the periodic variation of the inclination of such planar chains.

In the high-temperature α-phase this periodic variation of the inclination is absent for all zig-zag chains being situated in planes parallel to $(0001)_\alpha$ (Fig. 10a). It is reasonable to assume that the β-phase has some intermediate structure between the α- and γ-phase consisting of strips of γ-phase limited by planes parallel to $(010)_\gamma$. In the interface region the arrangement is α-like, as represented schematically in Fig. 11.

The presence of such a singular α-like planar arrangement causes a relative shift of the γ-structure on both sides of it over a vector $R = 1/4[010]$ which is in agreement with the observed R vector. The magnitude of the q vector suggests that in direct space the separation of such α-like planes should on the average be slightly less than four columns wide, which is somewhat less than the corresponding period of the γ-phase. This can be achieved by inserting, at regular intervals, singular layers separated by three columns rather than by four as in γ-phase (Fig. 11).

The fractional shift method only provides a geometrical building principle of the interface modulated

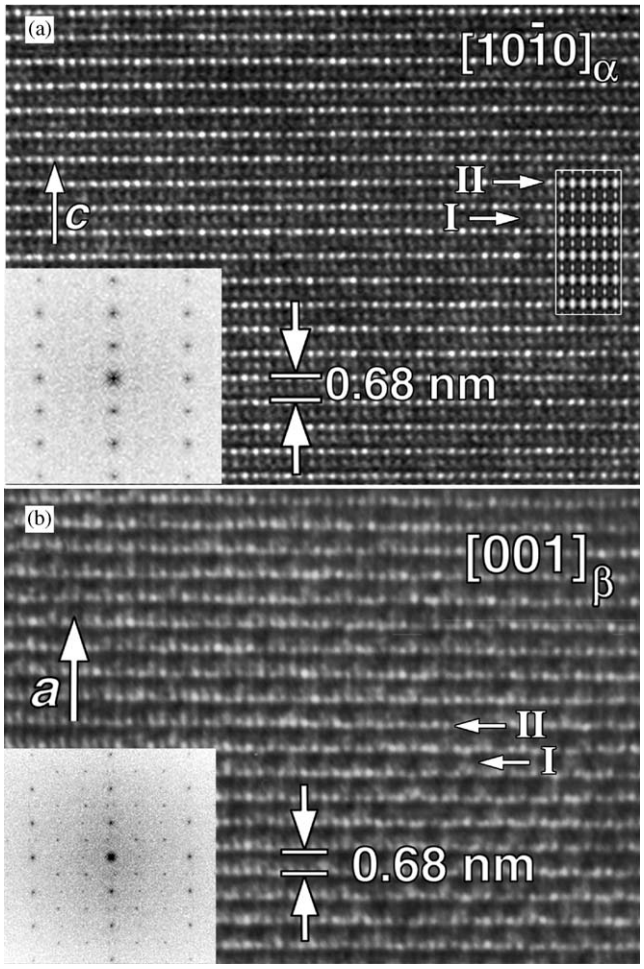

Fig. 13. HREM images of α- (a) and β-$K_5Yb(MoO_4)_4$ (b) along the [10$\bar{1}$0] and [001] zones, respectively. The calculated image of α-$K_5Yb(MoO_4)_4$ for a defocus value $\Delta f = -60$ nm and a thickness $t = 6$ nm is given as inset in (a). Layers corresponding to AO_4 tetrahedra (layer I) and M_2O_{10} polyhedra (layer II) in Fig. 10 are marked by arrows.

structure. If the basic structure is a simple one, this is usually sufficient to propose a detailed structure, as for example in long period antiphase boundary modulated superstructures based on the fcc lattice [24]. However, in the present case the "basic" structure is complex and one can only expect to find the building principle of the superstructure.

It should be noted that in the present case the "interfaces" result from the presence of a layer in the high-temperature α-configuration causing a relative displacement of two successive strips of γ-phase. The superstructure can also be considered as a deformation modulated structure of the α-phase.

The proposed β-phase model is essentially an interface modulated derivative of the γ-phase; the relative displacement of successive "modules" of the structure being caused by a phase shift of the inclination pattern of the pairs of K-ions. The incommensurability is

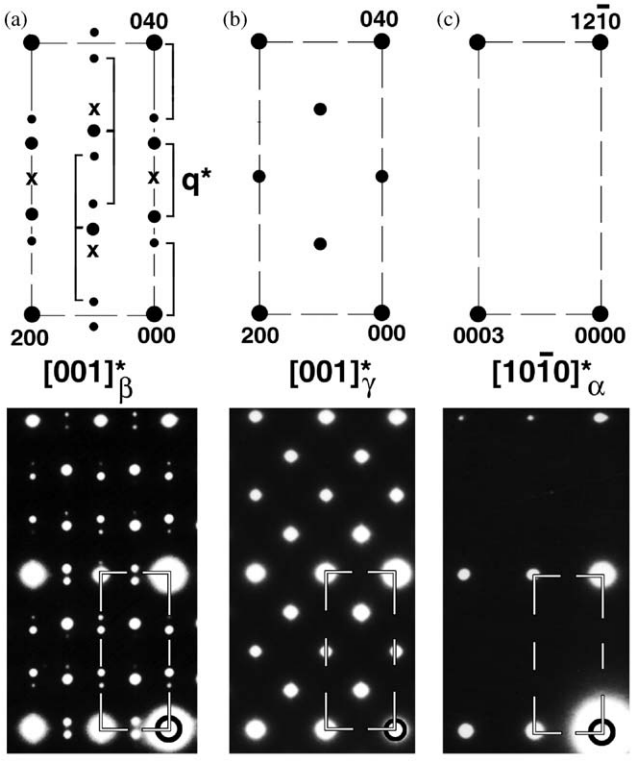

Fig. 14. Comparison of the ED patterns for α-, β- and γ-$K_5Yb(MoO_4)_4$.

obtained as a regular mixing of different spacings between such interfaces. The structure is clearly intermediate between that of the α- and of the γ-phase and is consistent with the thermal treatment required to form the β-phase, which is very unstable under e-irradiation.

The β-phase can also be described as related to the α-phase by the sinusoidal modulation of the inclination of the K-pairs. Modulation waves in successive layers have then to be in anti-phase so as to cause the observed centering along $[001]_\gamma$ in the diffraction pattern of the β-phase.

Acknowledgments

The authors are grateful to A.V. Mironov (Department of Chemistry, Moscow State University) for help with the X-ray experiments and to S.N. Mudretsova (Department of Chemistry, Moscow State University) for help with the DSC measurements. V.A. Morozov is grateful to DWTC (Belgium) for financial support. This work is performed within the framework of IAP V-1. O.I. Lebedev is on leave from the Institute of Crystallography, Russian Academy of Science, 117333, Moscow, Russia.

References

[1] A.A. Kaminskii, S.E. Sarkisov, J. Bohm, P. Reiche, D. Schulze, R. Hecker, Phys. Status Solidi 43a (1977) 71.
[2] G. Huber, W. Lentch, J. Lieberts, F. Lutz, J. Lumin. 16 (1978) 353.
[3] E.V. Vasil'ev, A.A. Evdokimov, V.A. Efremov, B.I. Lazoryak, V.F. Papulovskii, R.K. Sviridova, A.F. Solokha, V.K. Trunov, Rus. J. Appl. Spectr. 29 (1978) 846.
[4] M. Maeda, K. Sukiyama, T. Ikeda, Jpn. J. Appl. Phys. 18 (1979) 25.
[5] O.M. Basovich, E.G. Khaikina, S.F. Solodovnikov, Zh. Neorgan. Khim. 5 (2000) 1726 (Russian).
[6] B.I. Lazoryak, V.A. Efremov, Crystallogr. Rep. 32 (1978) 378.
[7] H.G. Bachmann, W. Kleber, Fortsch. Mineral. 31 (1952) 9.
[8] C.K. Möller, Acta Chem. Scand. 8 (1954) 81.
[9] R.F. Klevtsova, L.A. Glinskaya, Dokl. Akad. Nauk USSR 230 (1976) 1337 (Russian).
[10] P.V. Klevtsov, L.P. Kozeeva, V.I. Protasova, L.Yu. Kharchenko, L.A. Glinskaya, V.V. Bakakin, Crystallogr. Rep. 20 (1975) 57 (Russian).
[11] E.F. Dudnik, E.V. Sinyakov, Russ. Izv. Akad. Nauk USSR Ser. Phys. 41 (1977) 663 (Rusian).
[12] L.H. Brixner, P.E. Bierstedt, W.F. Jaep, J.R. Barkley, Mater. Res. Bull. 8 (1973) 497.
[13] J. Barbier, D. Maxin, J. Solid State Chem. 116 (1995) 179.
[14] A.I. Baranov, V.M. Duba, D.J. Jones, J. Roziere, V.V. Sinitsyn, R.C.T. Slade, Solid State Ionics 145 (2001) 241.
[15] H.M. Rietveld, Acta Crystallogr. 22 (1967) 151.
[16] F. Izumi, in: R.A. Young (Ed.), The Rietveld Method, Oxford University Press, New York, 1993 (Chapter 13).
[17] Y.-I. Kim, F. Izumi, J. Ceram. Soc. Jpn. 102 (1994) 401.
[18] A.C. Larson, R.B. Von Dreele, Generalized Crystal Analysis System (GSAS), LAUR 86-748, Los Alamos, 1988, 150pp.
[19] S.Yu. Stefanovich, in: Proceedings of the European Conference on Lasers and Electro-Optics (CLEO-Europe'94), Amsterdam, 1994, p. 249.
[20] T.P. Ribakova, V.K. Trunov, Zh. Neorgan. Khim. 18 (1973) 484 (Russian).
[21] B.I. Lazoryak, V.A. Efremov, Crystallogr. Rep. 26 (1981) 464.
[22] O.V. Kudin, V.A. Efremov, V.K. Trunov, Zh. Neorgan. Khim. 26 (1981) 2734 (Russian).
[23] S. Amelinckx, D. Van Dyck, in: J.M. Cowley (Ed.), Electron Diffraction Techniques, Vol. 2, Oxford University Press, New York, 1993, p. 309.
[24] G. Van Tendeloo, S. Amelinckx, Phys. Status Solidi 65 (1981) 73.